Electronic Supplementary Material (ESI) for Chemical Communications.

Supplementary information

Two-dimensional superlattice membrane enables high-performance desalination and enhanced Li ion selectivity

Lvyang Cheng,‡[a] Lei Dong,‡*[a] Yinjie Lv,[a] Tianyi Gao,[a] Yingjie He,[a] Cong Wu,[a] Xin Chen,[a] Yue Zhang, [a] Wenbo Zhai, [a] Yuanyuan Cui,*[b] Wei Liu *[a]

[a] School of Physical Science and Technology, ShanghaiTech University, Shanghai 201210, China

E-mail: liuwei1@shanghaitech.edu.cn, donglei@nwpu.edu.cn

[b]School of Materials Science and Engineering, Shanghai University, Shanghai 200444, China.

E-mail: cui-yy@shu.edu.cn

Acknowledgement

L.C. and L.D. carried out the experiments, characterizations, data analysis, and manuscript preparation. Y.H. conducted the SEM. C.W. conducted the depth-profiled XPS. T.G helped to draw figure in Materials Studio. Y.L. helped to prepare samples. Y.C. calculated GO-MoS_2 system in VASP by DFT. L.D. and W.L. managed the project, reviewed the results, and conducted data analysis and manuscript preparation.

The authors gratefully acknowledge financial support from ShanghaiTech setup funding, National Natural Science Foundation of China (51972206). We also acknowledge the Center for High resolution Electron Microscopy (CℏEM), SPST of ShanghaiTech University (#EM02161943), Shanghai Science and Technology Plan (21DZ2260400), for support.

Contents:

1. Scheme and Figures

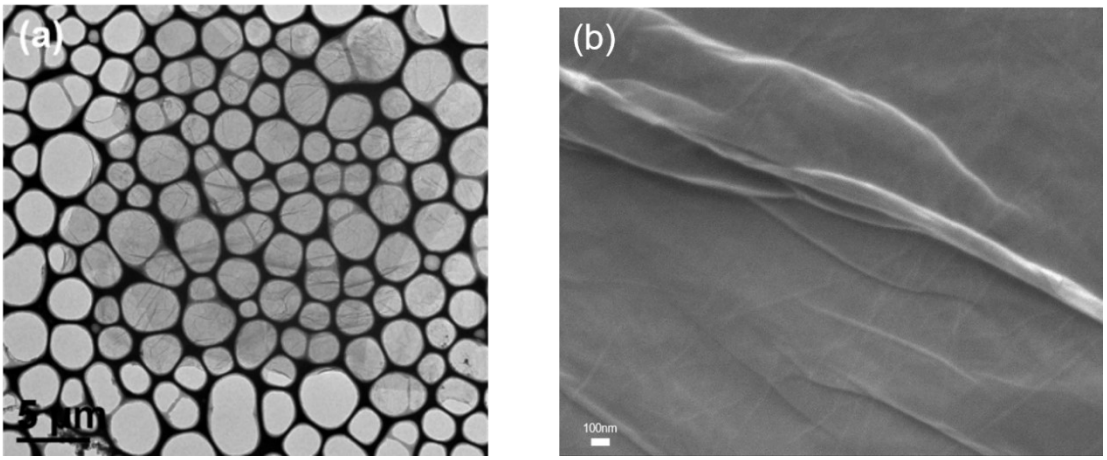

Figure S1. TEM image of GO nanosheet and (b) top side SEM of GO.

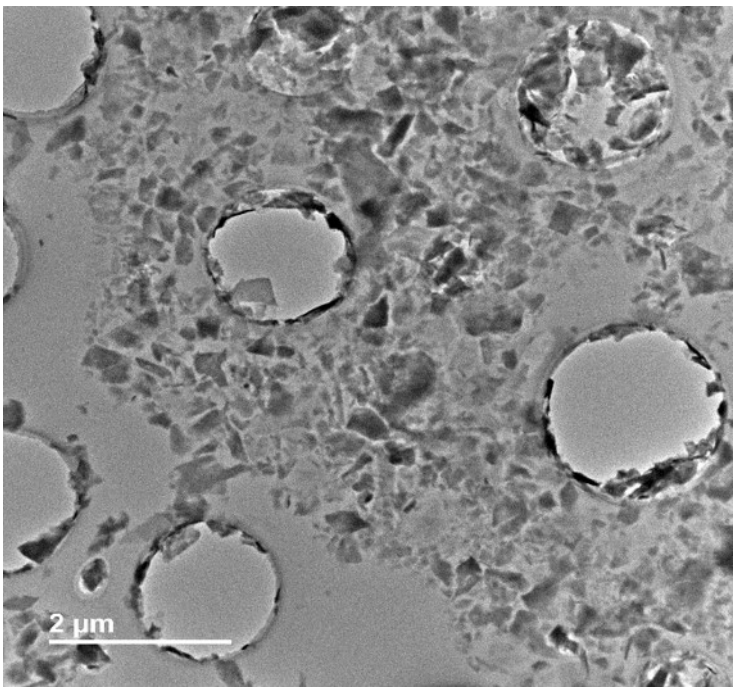

Figure S2. TEM image of MoS_2 nanosheets.

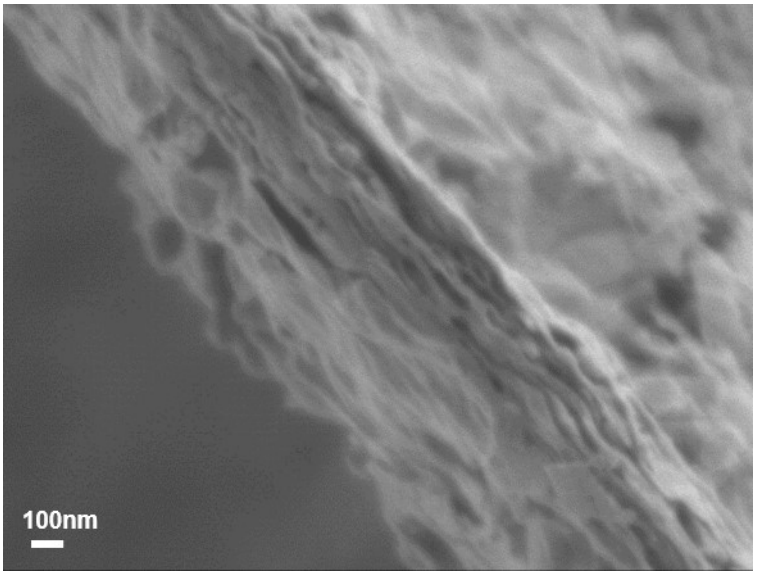

Figure S3. SEM image of GO-MoS_2 shows layer-stacked superlattice structure.

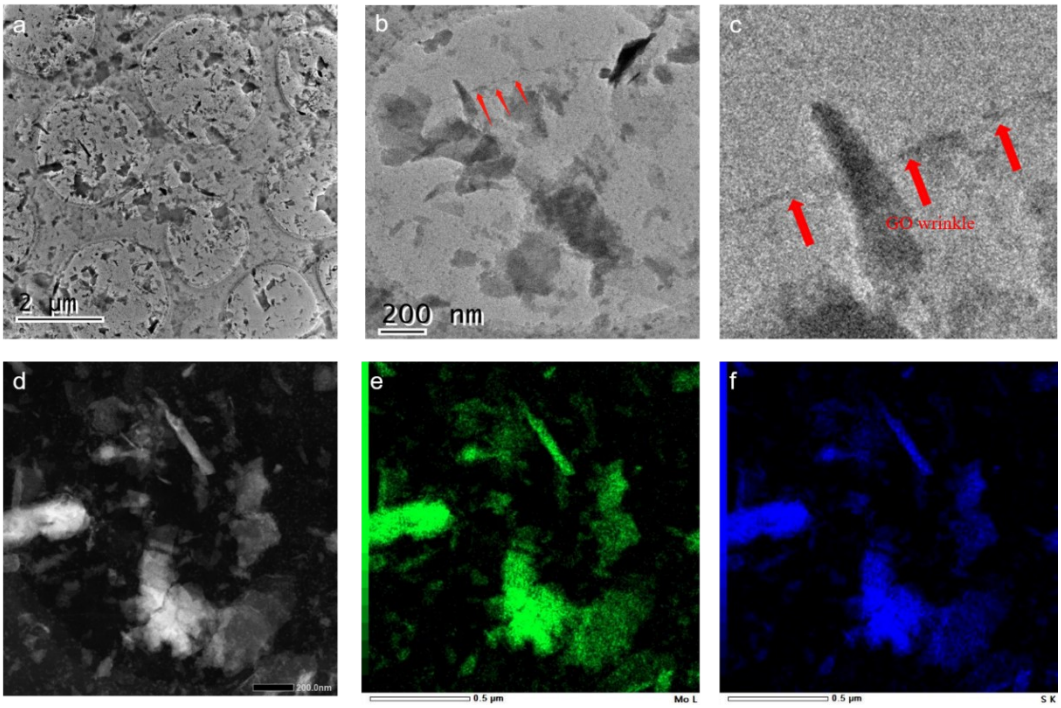

Figure S4. (a-c) TEM images of assembled GO-MoS_2 nanosheets. A drop of GO-MoS_2 mixture solution was added on the Cu grid for characterization. Here, small-sized MoS_2 nanosheets (< 0.5 μm) are loaded onto large-sized GO nanosheet (> 10 μm). Winkles of GO was marked because of the low-contrast of single-layered GO sheet. (d-f) EDS mapping of Mo (e) and S (f) elements. The corresponding TEM image is shown in d.

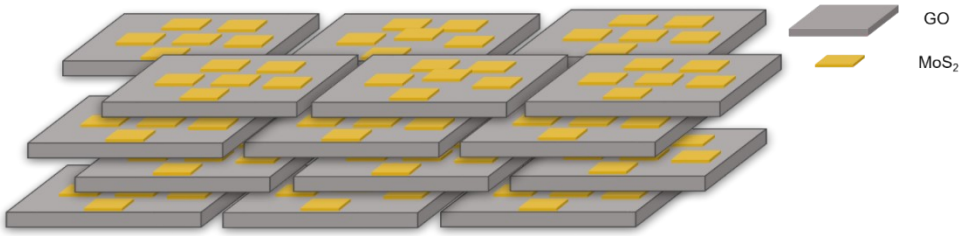

Figure S5. Schematic illustration of the self-assembled GO-MoS_2 superlattice membrane.

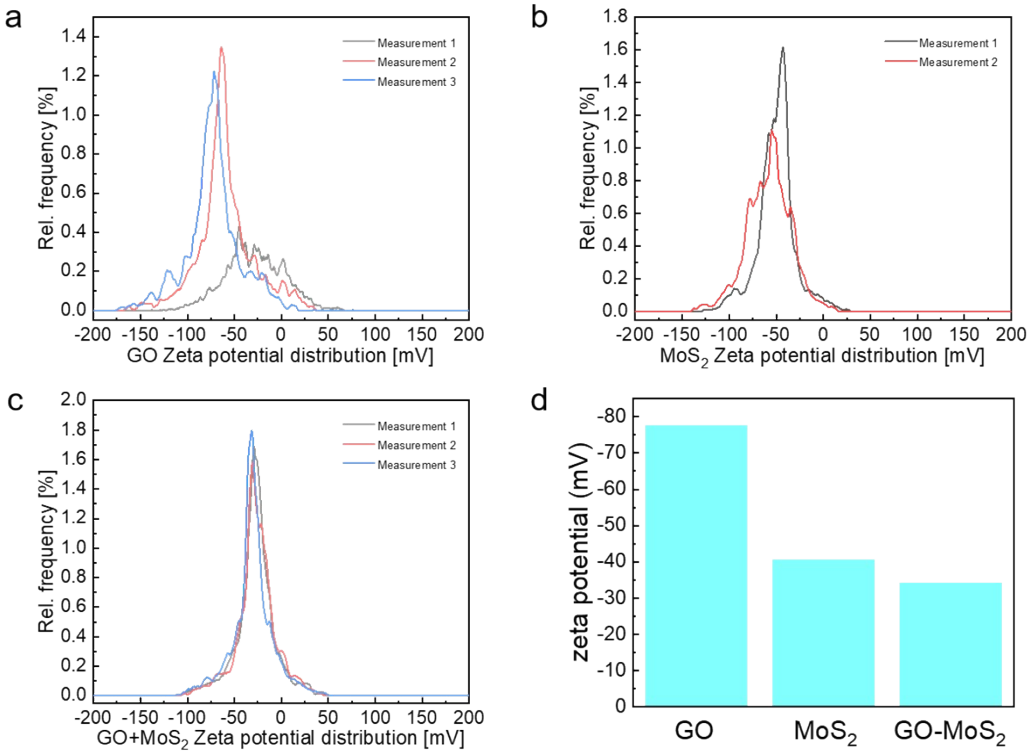

Figure S6. Zeta potential of GO (a), MoS_2 (b) and GO-MoS_2 (c) before filtration.

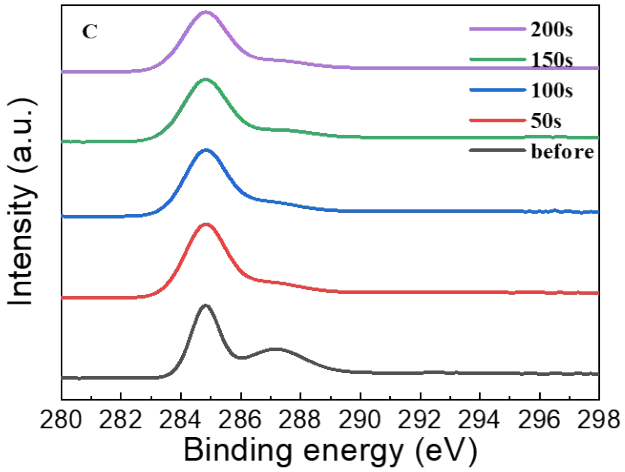

Figure S7. Depth-profiled XPS of Carbon curves with an etching rate of ~2 nm per 10 s.

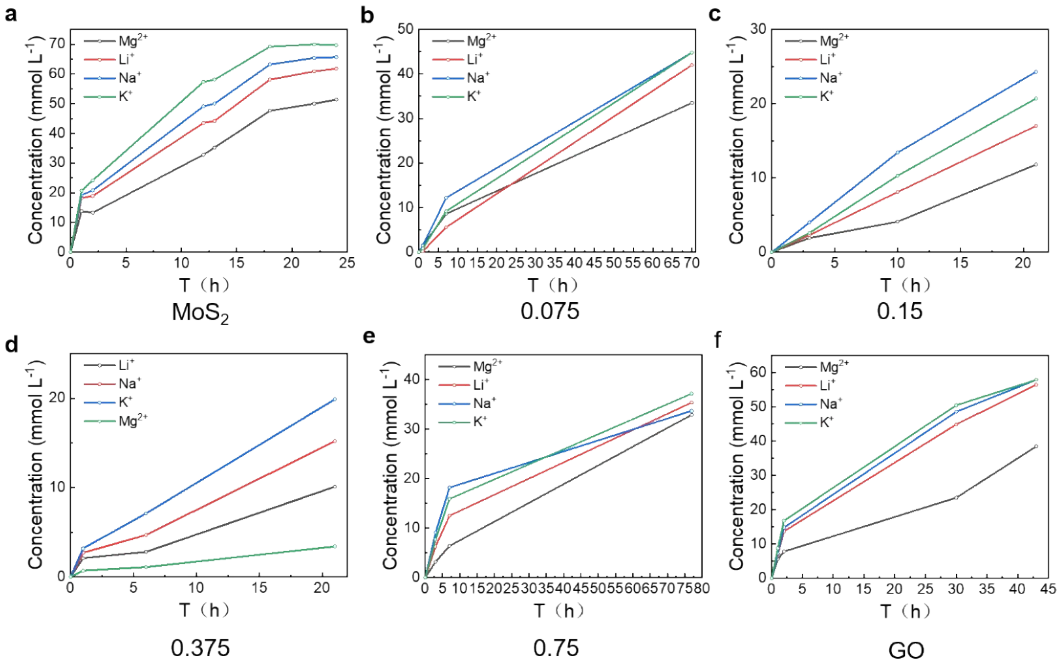

Figure S8. Water side concentration of GO-MoS_2 membranes with different MoS_2/GO ratio (based on the molar ratio of MoS_2 and C units).

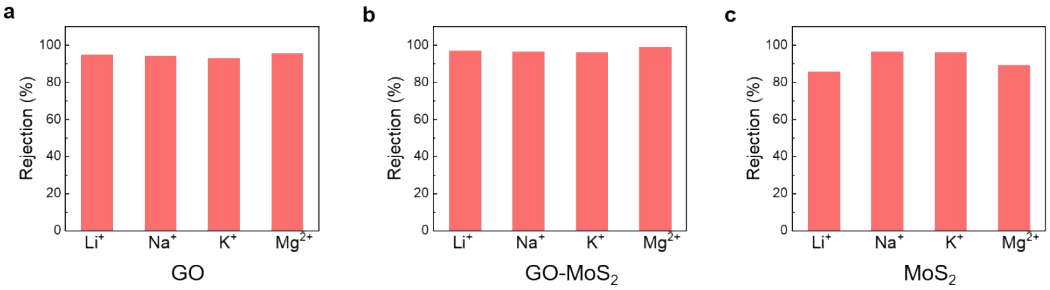

Figure S9. Rejections comparison for different ions indicate excellent desalination performance of GO-MoS_2 membrane.

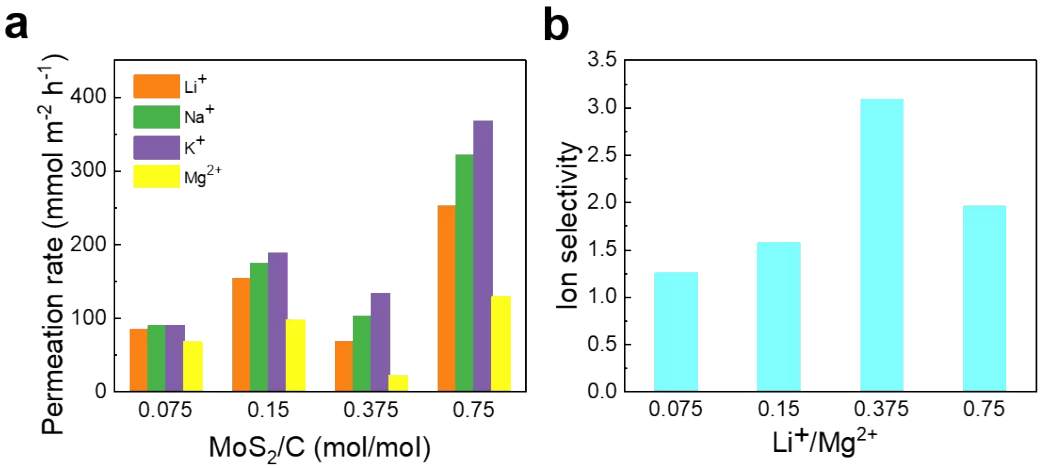

Figure S10. (a,b) Ion permeation rate of GO-MoS_2 membranes with different MoS_2/GO ratio (based on the molar ratio of MoS_2 and C units), (a) and the corresponding Li^+/Mg^{2+} ratio (b).

Table S1. Physical properties of ions studied in our work [1-3].

Ion	Bare diameter (Å)	Hydrated diameter (Å)
Li^+	1.20	7.64
Na^+	1.90	7.16
K^+	2.66	6.62
Mg^{2+}	1.30	8.56

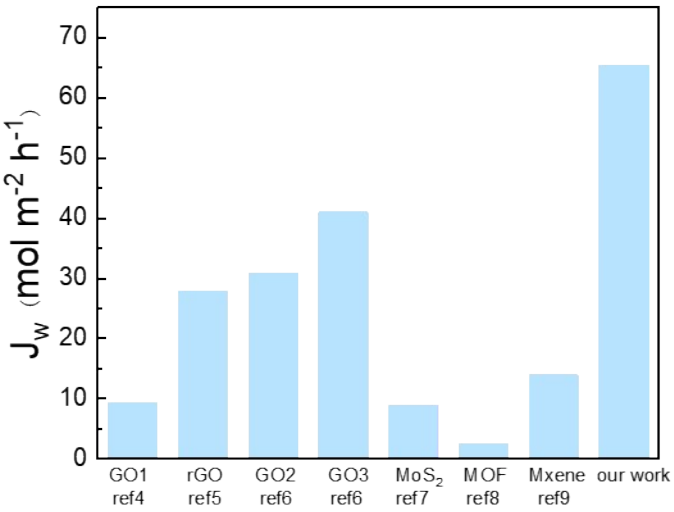

Figure S11. The comparison of water flux for the GO-MoS_2 membrane with reported publications [4-9].

Table S2. Comparison of 2D membranes and polyamide membranes [4-14] (forward osmotic pressure is calculated by Van't Hoff equation (Δπ).

Membrane materials	Operation mode	Δπ (bar)	J_w (mol m^{-2} h^{-1})	J_w/Δπ (mol m^{-2} h^{-1} bar^{-1})	J_s (salts pieces) (mmol m^{-2} h^{-1})	Selectivity (J_{SLi+}/J_{SMg2+})	Ref.
GO-MoS_2	Forward osmosis	21.92	65.4	2.98	68.0 (NaCl)	3.08	Our work
GO1	Forward osmosis	12	9.44	0.79	190 (NaCl)	n/a	[4]
rGO	Forward osmosis	75	27.8	0.37	n/a	n/a	[5]
GO2	Forward osmosis	24.46	30.83	1.26	6.11 (NaCl)	n/a	[6]
GO3	Forward osmosis	24.46	41.07	1.68	13.8 (NaCl)	n/a	[6]
MoS_2	Forward osmosis	75	9	0.12	860 (NaCl)	0.63	[7]
MOF	Forward osmosis	24	2.44	0.10	0.15 (NaCl)	n/a	[8]
MXene	Forward osmosis	4.89	13.93	2.86	6.7 (NaCl)	n/a	[9]
MCPM	Reverse osmosis	2	750.06	375.03	n/a	43.9	[10]
PA	Reverse osmosis	20	3000	150	n/a	n/a	[11]
AQP/PA	Reverse osmosis	5	2222.4	444.5	n/a	n/a	[12]
PA/SWCNT	Reverse osmosis	6	13334.4	2222.4	n/a	n/a	[13]
PA50/CNC/PES	Reverse osmosis	6	1133.2	1889	n/a	n/a	[14]

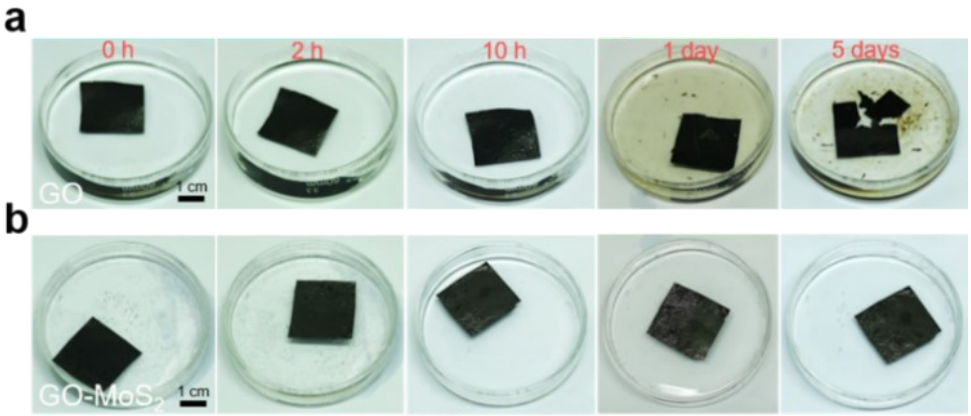

Figure S12. (a,b) Compared with GO membrane, GO-MoS_2 membrane shows significantly enhanced stability when immersing in water at 40 ℃. The two samples were mildly shaken in every 5 hours.

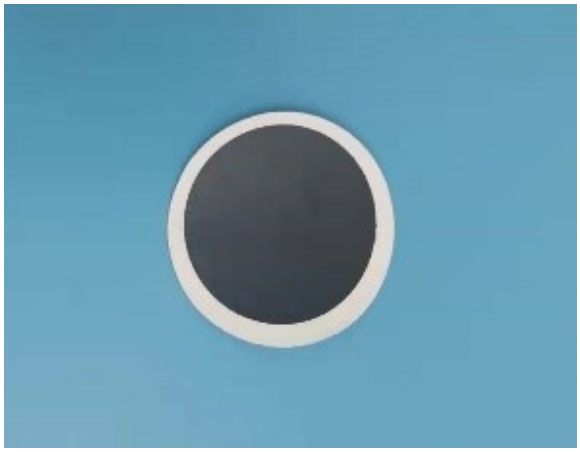

Figure S13. The photo of complete MoS_2-GO film.

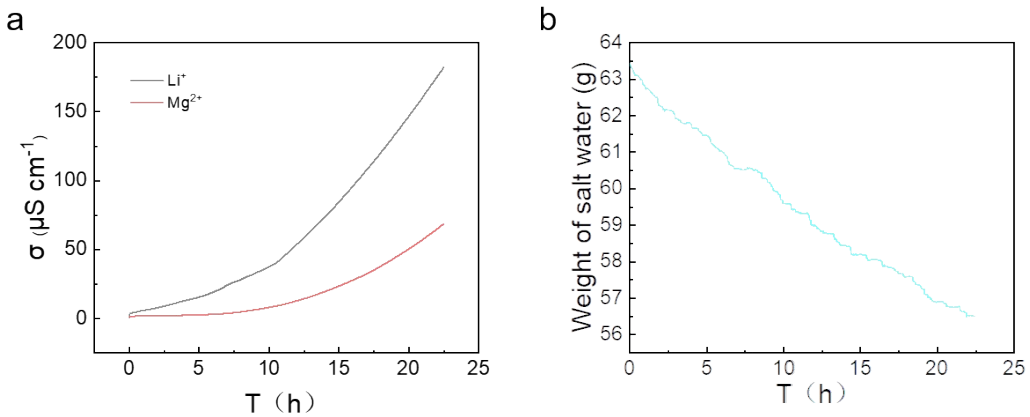

Figure S14. The conductivity and weight of salt water.

2. Experimental Section

2.1 Fabrication of GO-MoS_2 superlattice-structured membranes.

GO was prepared according to our previous report [15-18]. MoS_2 nanosheet dispersion (1 mg mL^{-1}) was purchased from XFNANO, INC (Nanjing, China). The MoS_2 nanosheets were dispersed in absolute ethanol by ultrasonic exfoliation for 30 min. Then the supernatant MoS_2 dispersion was obtained through centrifugation at 3000 rpm for 30 min. GO-MoS_2 membrane was prepared by a simple process where MoS_2 nanosheets dispersion was added dropwise into large-sized GO nanosheets dispersion and subsequently stood for self-assembly. Then superlattice-structured GO-MoS_2 membrane was formed after vacuum filtration and drying. The membranes' nylon hydrophilic bases were purchased from Titan.

2.2 Rejections and Desalination Performance Evaluation.

The water flux (J_w) was derived from the difference of liquid volume on the permeate side or the draw side (ΔV) with time (Δt) as following equation. The feed solution is the side with salt to provide osmotic pressure. The draw solution is the side with deionized water. While A (m^2) refers to the effective filtration area, Δt (h) is the filtration time.

$$J_w = \frac{\Delta V}{A \times \Delta t} \quad (1)$$

The ion permeation rate (J_s) through membranes could be calculated as the following equation

$$J_s = \frac{C \times V}{A \times \Delta t} \quad (2)$$

where C is the concentration of salt in the draw side, V is the total volume of draw solution, A is the effective membrane area, and Δt is the permeation time. The rotation speed of the magnetic stirrers in both sides was set up at 250 rpm to minimize concentration polarization. The feed solution is the side with salt to provide osmotic pressure. The draw solution is the side with deionized water.

$$R = \frac{C_0 - C}{C_0} \times 100\% \quad (3)$$

C_0 and C are the salt concentrations of the feed and draw solutions, respectively.

A set of home-made, H-type cell (volume 50 mL) was employed for liquid filtration test (Figure 4a). Our GO-MoS_2 membrane was fixed between the feed and permeate compartments by two O-rings to provide a leakfree environment. And 50 ml of 0.1 M salt (NaCl or $MgCl_2$) aqueous solution and deionized water were filled into feed

and permeate compartments, respectively. All solutions were under stirring at 250 rpm and room temperature. The permeated salts were measured using Inductively coupled plasma optical emission spectrometer (ICP-OES) on an iCAP 7400 Radial.

2.3 Characterizations.

XRD was performed on a Bruker D8 Advance using a Cu Kα (λ = 1.5418 Å) radiation source. Small angle x-ray scattering system (SAXS) was performed on a Xenocs 2.0 using a Cu GeniX3D radiation source with a Pilatus 3 100K/300K detector. Inductively coupled plasma optical emission spectrometer (ICP-OES) was conducted on an iCAP 7400 Radial. SEM patterns were recorded using a JEOL JSM-7800F. Transmission electronmicroscopy (TEM) observation was conducted using a JEOL F200 equipped with a field emission gun. XPS spectra was recorded with the ThermoFisher ESCA 250XI using an Al Kα (λ = 0.83 nm, hυ = 1486.7 eV). And, the X-ray source was operated at 2 kV, 20 mA. Profile XPS was conducted using Tantalum oxide (Ta_2O_5) with a sputter rate of 10 nm/min.

2.4 Computational methods

The calculation of first principle theory is supported by the Vienna ab initio simulation package (VASP). The projected augmented wave potentials (PAW) [19] was chosen to describe the ionic cores. And the exchange-correlation part of the density functional was conducted by the generalized gradient approximation (GGA) of Perdew-Burke-Ernzerhof (PBE)[20]. The convergence criteria were set to 0.01 eV $Å^{-1}$ and 10^-5 eV for the residual force and energy during structure relaxation.

The equilibrium lattice constants of MoS_2/GO heterogeneous were optimized to be a=12.40 Å, b=12.40 Å and c=11.3 Å. These lattice constants were used to build the MoS_2 (001) surface slab with 1 atomic layers, which contains 16 Mo and 32 S atoms, and the C (002) surface slab with 1 atomic layers, which contains 50 C atoms. During structural optimizations of the models, a 3×3×1 gamma-point centered k-point grid for Brillouin zone was used and all the atoms were allowed to fully relax.

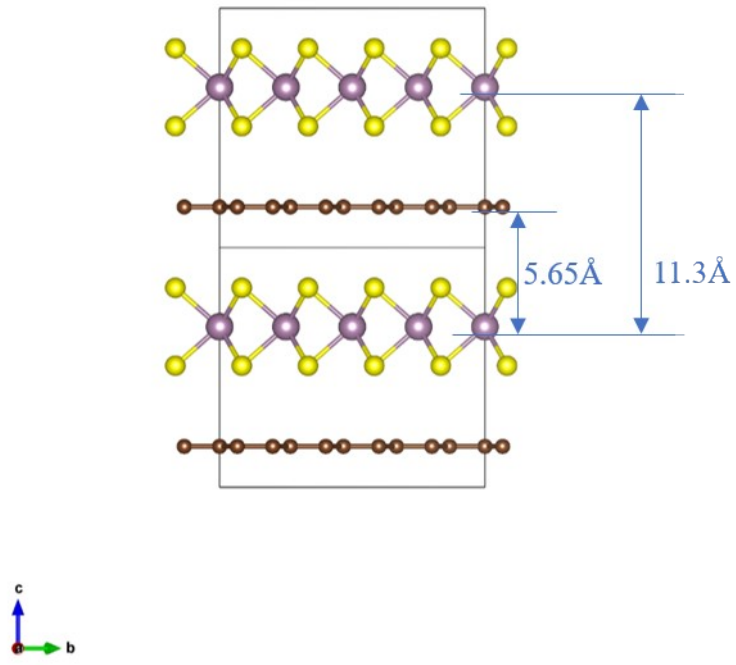

Figure S15. The structure of MoS_2/GO.

The binding energy of M (M = Na, K, Li, Mg) was defined as:

$$E_V = E_b - E_p - E_A \quad (4)$$

Where E_b, E_p and E_A are the energy of the MoS_2-M-GO sandwich structure, the energy of MoS_2-GO, and the energy of M atom in the lattice, respectively.

The difference in the spacing between the layers of molybdenum disulfide and graphene oxide in the experiments and first-principles calculations can be explained by the difference in functional groups. GO is used in actual experiments, which has oxygen atoms, hydroxyl groups and carboxyl groups on its surface. The polarity introduced by these functional groups and their volume will increase the distance between the two sides.

References

1 H. Binder and O. Zschornig, *Chem. Phys. Lipids*, 2002, **115**, 39-61.

2 B. E. Conway and E. Ayranci, *Journal of Solution Chemistry*, 1999, **28**, 163-192.

3 A. G. Volkov, S. Paula and D. W. Deamer, *Bioelectrochemistry and Bioenergetics*, 1997, **42**, 153-160.

4 L. Chen, G. Shi, J. Shen, J. Li and H. Fang, *Nature*, 2017, **550**, 380-383.

5 J. Abraham, K. S. Vasu, C. D. Williams, K. Gopinadhan, Y. Su, C. T. Cherian, J. Dix, E. Prestat, S. J. Haigh, I. V. Grigorieva, P. Carbone, A. K. Geim and R. R. Nair, *Nat. Nanotechnol.*, 2017, **12**, 546.

6 Y. Qian, J. Shang, D. Liu, G. Yang, X. Wang, C. Chen, L. Kou and W. Lei, *J. Am. Chem. Soc.*, 2021, **143**, 5080-5090.

7 M. Deng, K. Kwac, M. Li, Y. Jung and H. G. Park, *Nano Lett.*, 2017, **17**, 2342-2348.

8 M. P. Jian, R. S. Qiu, Y. Xia, J. Lu, Y. Chen, Q. F. Gu, R. P. Liu, C. Z. Hu, J. H. Qu, H. T. Wang and X. W. Zhang, *Sci. Adv.*, 2020, **6**.

9 Z. Lu, Y. Y. Wei, J. J. Deng, L. Ding, Z. K. Li and H. H. Wang, *Acs Nano*, 2019, **13**, 10535-10544.

10 J. Zhao, X. You, G. Wang, J. Yuan, Y. Li, C. Yang, S. Zhang, X. Wang, R. Zhang, H. Wu and Z. Jiang, *J. Membrane Sci.*, 2022, **644**.

11 Z. Jiang, S. Karan and A. G. Livingston, *Adv. Mater.*, 2018, **30**, e1705973.

12 X. Li, S. Chou, R. Wang, L. Shi, W. Fang, G. Chaitra, C. Y. Tang, J. Torres, X. Hu and A. G. Fane, *J. Membrane Sci.*, 2015, **494**, 68-77.

13 S. Gao, Y. Zhu, Y. Gong, Z. Wang, W. Fang and J. Jin, *ACS Nano*, 2019, **13**, 5278-5290.

14 J.-J. Wang, H.-C. Yang, M.-B. Wu, X. Zhang and Z.-K. Xu, *J Mater. Chem. A*, 2017, **5**, 16289-16295.

15 J. Zhang, Q. Liu, Y. Ruan, S. Lin, K. Wang and H. Lu, *Chem. Mater.*, 2018, **30**, 1888-1897.

16 L. Dong, Z. Chen, S. Lin, K. Wang, C. Ma and H. Lu, *Chem. Mater.*, 2017, **29**, 564-572.

17 L. Dong, J. Yang, M. Chhowalla and K. P. Loh, *Chem. Soc. Rev.*, 2017, **46**, 7306-7316.

18 L. Dong, L. Zhang, S. Lin, Z. Chen, Y. Wang, X. Zhao, T. Wu, J. Zhang, W. Liu, H. Lu and K. P. Loh, *Nano Energy*, 2020, **70**, 104482.

19 G. Kresse and J. Furthmüller, *Phys. Rev. B*, 1996, **54**, 11169–11186.

20 John P. Perdew, Kieron Burke and a. M. Ernzerhof, *Phys. Rev. Lett.*, 1996, **77**, 3865–3868.